Deformation due to a pressurized horizontal circular crack in an elastic half-space, with applications to volcano geodesy

Yuri Fialko,[1,]* Yakov Khazan[2] and Mark Simons[3]

[1] *Seismological Laboratory, California Institute of Technology, Pasadena, CA 91125, USA. E-mail: fialko@gps.caltech.edu*
[2] *Department of Tectonophysics, Institute of Geophysics, Kiev, 252680, Ukraine. E-mail: khazan@igph.kiev.ua*
[3] *Seismological Laboratory, California Institute of Technology, Pasadena, CA 91125, USA. E-mail: simons@caltech.edu*

SUMMARY

We consider deformation due to sill-like magma intrusions using a model of a horizontal circular crack in a semi-infinite elastic solid. We present exact expressions for vertical and horizontal displacements of the free surface of a half-space, and calculate surface displacements for a special case of a uniformly pressurized crack. We derive expressions for other observable geophysical parameters, such as the volume of a surface uplift/subsidence, and the corresponding volume change due to fluid injection/withdrawal at depth. We demonstrate that for essentially oblate (i.e. sill-like) source geometries the volume change at the source always equals the volume of the displaced material at the surface of a half-space. Our solutions compare favourably to a number of previously published approximate models. Surface deformation due to a 'point' crack (that is, a crack with a large depth-to-radius ratio) differs appreciably from that due to an isotropic point source ('Mogi model'). Geodetic inversions that employ only one component of deformation (either vertical or horizontal) are unlikely to resolve the overall geometry of subsurface deformation sources even in a simplest case of axisymmetric deformation. Measurements of a complete vector displacement field at the Earth's surface may help to constrain the depth and morphology of active magma reservoirs. However, our results indicate that differences in surface displacements due to various axisymmetric sources may be subtle. In particular, the sill-like and pluton-like magma chambers may give rise to differences in the ratio of maximum horizontal displacements to maximum vertical displacements (a parameter that is most indicative of the source geometry) that are less than 30 per cent. Given measurement errors in geodetic data, such differences may be hard to distinguish.

Key words: displacement, intrusion, magma, modelling, sill, theory.

1 INTRODUCTION

Geodetic observations in many neovolcanic areas reveal episodes of uplift and subsidence of the Earth's surface that have been attributed to migration of magma or other geological fluids at depth (e.g. Mogi 1958; Davis 1986; Savage *et al.* 1987; Dvorak & Dzurisin 1997). Inferred ground deformations often exhibit a nearly axisymmetric pattern (e.g. Savage *et al.* 1987; Bianchi *et al.* 1987; Dzurisin & Yamashita 1987; Lanari *et al.* 1998). These observations are commonly interpreted in terms of a point pressure source at depth ('Mogi model'). The Mogi model physically represents a uniformly pressurized spherical cavity in an elastic half-space (Mogi 1958; McTigue 1987). This

model gained much popularity in volcano geodesy because it has a simple analytical solution for surface displacements, and in many cases does a reasonably good job of explaining field observations. However, recent advances in quality and quantity of geodetic measurements (in particular, the advent of satellite-based techniques such as the Global Positioning System and Interferometric Synthetic Aperture Radar) motivate more detailed studies of the morphology and dynamics of the inferred deformation sources. Interpretations of geodetic data hinge upon the availability of accurate and computationally efficient models of geologically reasonable mechanisms of deformation. In particular, realistic models of magma-induced deformation are of great importance for forecasts of volcanic and seismic hazards in regions of contemporaneous magmatic activity (e.g. Gudmundsson 1986; Bianchi *et al.* 1987; Dvorak & Dzurisin 1997).

*Now at: Institute of Geophysics and Planetary Physics, UCSD, La Jolla, CA 92093, USA. E-mail: fialko@radar.ucsd.edu

During the last two decades, significant progress has been made in the development of theoretical models of deformation due to subsurface fluid reservoirs. Davis (1986) has generalized the Mogi model to a case of an anisotropic point source. Yang *et al.* (1988) have offered approximate solutions for a finite uniformly pressurized prolate cavity in an elastic half-space. These solutions have been successfully used to interpret ground deformation due to a number of geological and man-made processes (e.g. Wu & Wang 1988; Linde *et al.* 1993; Fialko & Simons 2000). In this paper we consider a model of surface deformation due to magma injection into (or withdrawal from) a finite oblate cavity (i.e. a magma sill). In a companion paper (Fialko *et al.* 2001) we apply this model to study magma-induced deformation in areas of active crustal magma bodies in Socorro, New Mexico, and Long Valley, California.

2 PREVIOUS MODELLING WORK

A number of elastic solutions have been proposed to describe deformations associated with sill-like magma intrusions. The two-dimensionality of sheet intrusions such as sills and dykes allows one to treat them as fluid-pressurized cracks in an elastic medium (e.g. Pollard & Segall 1987). This is because strains induced by magma-driven fractures are of the order of the intrusion aspect ratio (the ratio of a characteristic thickness to a characteristic length), and therefore are small everywhere except for in a limited region near the fracture tip (e.g. Khazan & Fialko 1995). Therefore, it is reasonable to expect that the bulk of the host rock behaves essentially elastically on a time-scale of an intrusion event. Early models of deformation due to magma fractures considered dilational fluid-filled cracks in an infinite elastic solid (Anderson 1938; Pollard 1973). Pollard & Holzhausen (1979) presented theoretical solutions for a 2-D arbitrarily oriented slit in an elastic half-space and computed corresponding stress intensity factors at the tips of the slit, and displacements at the free surface of a half-space. Extension of these results to 3-D geometries proved to be difficult. Sun (1969) obtained approximate expressions for vertical displacements of the free surface due to a horizontal circular crack by superimposing a full-space solution and an auxiliary stress function that exactly satisfies traction-free boundary conditions at the surface of a half-space. However, such a superposition modifies prescribed boundary conditions at the crack surface. As shown in Section 4, this modification leads to significant errors in predicted displacements at the half-space surface when the crack radius becomes comparable to or exceeds the crack depth. Similar problem arises if an intrusion with a small depth-to-radius ratio is approximated by a dislocation (e.g. Davis 1983). In this case, errors in surface displacements result from unphysical boundary conditions at the intrusion surface (a constant displacement instead of a more realistic constant pressure). Also, dislocation models poorly resolve stresses near the crack tip, which limits their use in modelling of the crack growth. While stress and displacement fields due to cracks in an elastic half-space may be computed using numerical techniques (e.g. finite element or boundary element methods) given some adequate discretization of a problem, analytic solutions are warranted because of their accuracy and computational efficiency (the latter especially matters for inverse problems that require the generation of many forward models). Dieterich & Decker (1975) used a finite element model to compute ground surface displacements for a variety of axisymmetric magma

chamber shapes, including two sill-like geometries. As we shall demonstrate below, their results significantly overpredict the spatial extent of deformation, and somewhat underpredict horizontal displacements due to sills. Our model will be useful for benchmarking and calibration of 3-D numerical codes that are capable of handling complex loading geometries.

A simple 3-D model of a sill intrusion is a horizontal penny-shaped crack in a semi-infinite elastic body (Fig. 1). An axisymmetric elastic problem for a penny-shaped crack in a half-space has been considered in engineering mechanics (Kuzmin & Uflyand 1965; Srivastava & Singh 1969), but for a limited range of crack depth-to-radius ratios, and many aspects of the problem that are of geophysical interest (e.g. deformations at the surface of a half-space) have not been addressed. We use an approach developed by Guterman *et al.* (1996) to derive exact solutions for displacements of the free surface of a half-space due to an arbitrarily loaded axisymmetric crack, and numerically evaluate our solutions for an important special case of a uniformly pressurized crack. We also present expressions for the volume of a surface uplift/subsidence, and a corresponding volume change at depth due to magma injection/withdrawal at the source. Section 3 gives mathematical details of our solution. Readers who are not interested in these details may proceed to Section 4, which presents the results of our modelling.

3 SOLUTIONS FOR STRESSES AND DISPLACEMENTS DUE TO A PRESSURIZED HORIZONTAL CIRCULAR CRACK IN AN ELASTIC HALF-SPACE

Consider a horizontal penny-shaped crack with radius R and depth H in an elastic half-space (Fig. 1). The vertical axis in Fig. 1 is the axis of symmetry (positive downwards), with an origin at the crack centre. The surface of the half-space is assumed to be stress-free. The crack plane divides the half-space into two domains, as shown in Fig. 1. We anticipate self-similar solutions for stresses $\sigma_{jk}^{(i)}$ ($j=r, z$ and $k=r, z$, where r and z are spatial coordinates, and the index in parentheses corresponds to the upper and lower domains of a half-space, $i=1, 2$, see Fig. 1) and displacements $U_j^{(i)}$ that depend on the ratio of the crack depth H to the crack radius R, $h=H/R$. Accordingly, we normalize all variables having dimensionality of length with respect to the crack radius R, and all variables having dimensionality of pressure or stress with respect to the shear modulus of the elastic half-space μ. Thus, all variables below are non-dimensional, unless noted otherwise. The boundary conditions for the problem shown in Fig. 1 are as follows:
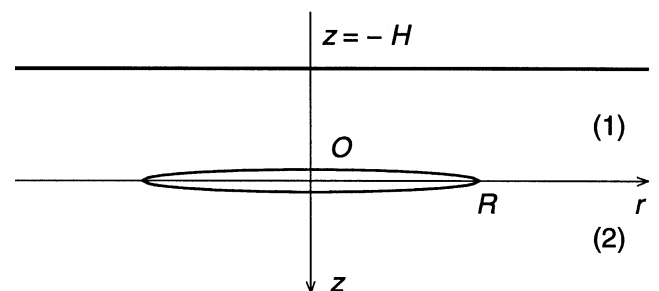

Figure 1. Schematic view of a horizontal circular crack in a semi-infinite elastic body.

for $z = -h$ (at the free surface),

$$\sigma_{zz}^{(1)} = \sigma_{rz}^{(1)} = 0 \quad \text{for} \quad 0 \le r < \infty\,; \tag{1}$$

for $z = 0$ (in the crack plane),

$$\sigma_{zz}^{(1)} = \sigma_{zz}^{(2)} = -\Delta p(r)\,,$$

$$\sigma_{rz}^{(1)} = \sigma_{rz}^{(2)} = \tau(r) \quad \text{for} \quad 0 \le r < 1\,, \tag{2}$$

$$U_z^{(1)} = U_z^{(2)}, \quad U_r^{(1)} = U_r^{(2)} \quad \text{for} \quad 1 \le r < \infty\,. \tag{3}$$

In eq. (2), $\Delta p(r)$ is the difference between the magma pressure and the lithostatic pressure, $\tau(r)$ is the shear stress at the crack walls, and we assume that the top and bottom crack faces have the same stress distribution. Compressive stresses are taken to be negative and tensile stresses are positive. In the case of an axial symmetry, solutions to the governing equations of the theory of elasticity may be expressed through two harmonic Papkovich–Neuber functions, $P^{(i)}$ and $N^{(i)}$, such that (e.g. Whittaker & Watson 1963)

$$2U_z^{(i)} = (3 - 4v)P^{(i)} - \frac{\partial N^{(i)}}{\partial z} - z\frac{\partial P^{(i)}}{\partial z}\,, \tag{4}$$

$$2U_r^{(i)} = -\frac{\partial N^{(i)}}{\partial r} - z\frac{\partial P^{(i)}}{\partial r}\,, \tag{5}$$

$$\sigma_{zz}^{(i)} = -\frac{\partial^2 N^{(i)}}{\partial z^2} + 2(1 - v)\frac{\partial P^{(i)}}{\partial z} - z\frac{\partial^2 P^{(i)}}{\partial z^2}\,, \tag{6}$$

$$\sigma_{rz}^{(i)} = -\frac{\partial^2 N^{(i)}}{\partial r \partial z} + (1 - 2v)\frac{\partial P^{(i)}}{\partial r} - z\frac{\partial^2 P^{(i)}}{\partial r \partial z}\,, \tag{7}$$

where v is Poisson's ratio. We wish to find functions $P^{(i)}$ and $N^{(i)}$ that satisfy eqs (4)–(7) and boundary conditions (1)–(3). We use a chain of integral transformations to reduce this problem to a system of integral Fredholm equations of the second kind that can be solved numerically (Kuzmin & Uflyand 1965; Srivastava & Singh 1969; Guterman *et al.* 1996). Harmonic functions $P^{(i)}$ and $N^{(i)}$ admit the following integral representation:

$$P^{(1)} = \int_0^\infty \left[A \operatorname{ch}\left(\xi(z + h)\right) + B \operatorname{sh}\left(\xi(z + h)\right) \right] J_0(\xi r) \frac{d\xi}{\operatorname{sh}(\xi h)}\,, \tag{8}$$

$$N^{(1)} = \int_0^\infty \left[C \operatorname{ch}\left(\xi(z + h)\right) + D \operatorname{sh}\left(\xi(z + h)\right) \right] J_0(\xi r) \frac{d\xi}{\operatorname{sh}(\xi h)}\,, \tag{9}$$

$$P^{(2)} = \int_0^\infty E e^{-\xi z} J_0(\xi r)\, d\xi\,, \tag{10}$$

$$N^{(2)} = -\int_0^\infty F e^{-\xi z} J_0(\xi r) \frac{d\xi}{\xi}\,, \tag{11}$$

where $\operatorname{sh}(x) = (e^x - e^{-x})/2$ is the hyperbolic sine, $\operatorname{ch}(x) = (e^x + e^{-x})/2$ is the hyperbolic cosine, J_0 is the Bessel function of the first kind and zero order, and A, B, C, D, E and F are arbitrary functions of ξ (representations for $P^{(2)}$ and $N^{(2)}$ are chosen such that the latter vanish at $z \to \infty$). It may be verified by direct substitution that expressions (8)–(11) satisfy the Laplace equation in cylindrical coordinates. Putting expressions (8)–(11) into equilibrium eqs (4)–(7) and making use of boundary conditions (1) to eliminate two unknowns C

and D, we obtain

$$2U_z^{(1)} = \int_0^\infty \left[\left((1 - 2v)B - \xi(z + h)A\right)\operatorname{sh}\left(\xi(z + h)\right) \right.$$
$$\left. + \left(2(1 - v)A - \xi(z + h)B\right)\operatorname{ch}\left(\xi(z + h)\right) \right] J_0(\xi r) \frac{d\xi}{\operatorname{sh}(\xi h)}\,, \tag{12}$$

$$2U_r^{(1)} = \int_0^\infty \left[\left((1 - 2v)A + \xi(z + h)B\right)\operatorname{sh}\left(\xi(z + h)\right) \right.$$
$$\left. + \left(2(1 - v)B + \xi(z + h)A\right)\operatorname{ch}\left(\xi(z + h)\right) \right] J_1(\xi r) \frac{d\xi}{\operatorname{sh}(\xi h)}\,, \tag{13}$$

$$\sigma_{zz}^{(1)} = \int_0^\infty \left[\left(A - \xi(z + h)B\right)\operatorname{sh}\left(\xi(z + h)\right) \right.$$
$$\left. - \xi(z + h)A\operatorname{ch}\left(\xi(z + h)\right) \right] J_0(\xi r) \frac{\xi d\xi}{\operatorname{sh}(\xi h)}\,, \tag{14}$$

$$\sigma_{rz}^{(1)} = \int_0^\infty \left[\left(\xi(z + h)A + B\right)\operatorname{sh}\left(\xi(z + h)\right) \right.$$
$$\left. + \xi(z + h)B\operatorname{ch}\left(\xi(z + h)\right) \right] J_1(\xi r) \frac{\xi d\xi}{\operatorname{sh}(\xi h)}\,, \tag{15}$$

$$2U_z^{(2)} = \int_0^\infty \left[E(3 - 4v + \xi z) - F \right] e^{-\xi z} J_0(\xi r)\, d\xi\,, \tag{16}$$

$$2U_r^{(2)} = \int_0^\infty \left[\xi z E - F \right] e^{-\xi z} J_1(\xi r)\, d\xi\,, \tag{17}$$

$$\sigma_{zz}^{(2)} = \int_0^\infty \left[F - \left(2(1 - v) + \xi z\right)E \right] e^{-\xi z} J_0(\xi r)\xi\, d\xi\,, \tag{18}$$

$$\sigma_{rz}^{(2)} = \int_0^\infty \left[F - \left((1 - 2v) + \xi z\right)E \right] e^{-\xi z} J_1(\xi r)\xi\, d\xi\,, \tag{19}$$

where J_1 is the Bessel function of the first kind and first order. From conditions (2) and formulae (14) and (18), and (15) and (19), respectively, we obtain the following relations between the remaining unknown functions:

$$(1 - a\operatorname{cth}(a))A - aB = F - 2(1 - v)E\,,$$

$$aA + (1 + a\operatorname{cth}(a))B = F - (1 - 2v)E\,, \tag{20}$$

where $a = \xi h$ and $\operatorname{cth}(x) = \operatorname{ch}(x)/\operatorname{sh}(x)$ is the hyperbolic cotangent. Note that eqs (20) automatically ensure continuity of stresses in the crack plane for $r > 1$. Using eqs (12), (13), (16) and (17), we find that in the crack plane ($z = 0$),

$$2(U_z^{(1)} - U_z^{(2)}) = \int_0^\infty \left[\left(2(1 - v)\operatorname{cth}(a) - a\right)A \right.$$
$$+ \left(1 - 2v - a\operatorname{cth}(a)\right)B$$
$$\left. - (3 - 4v)E + F \right] J_0(\xi r)\, d\xi\,,$$

$$2(U_r^{(1)} - U_r^{(2)}) = \int_0^\infty \left[\left(1 - 2v + a\operatorname{cth}(a)\right)A \right.$$
$$\left. + \left(a + 2(1 - v)\operatorname{cth}(a)\right)B + E \right] J_1(\xi r)\, d\xi\,. \tag{21}$$

We introduce new functions

$$4(1 - v)\Phi = \Big(2(1 - v)\mathrm{cth}(a) - a\Big)A$$

$$+ \Big(1 - 2v - a\,\mathrm{cth}(a)\Big)B - (3 - 4v)E + F,$$

$$4(1 - v)\Psi = \Big(1 - 2v + a\,\mathrm{cth}(a)\Big)A$$

$$+ \Big(a + 2(1 - v)\mathrm{cth}(a)\Big)B + E, \tag{22}$$

so that expressions (21) and the boundary conditions (3) for the continuity of displacements outside the crack (i.e. for $r > 1$) give rise to

$$\int_0^\infty \Phi(\xi)J_0(\xi r)d\xi = 0,$$

$$\int_0^\infty \Psi(\xi)J_1(\xi r)d\xi = 0. \tag{23}$$

Using relationships (20) and (22), functions A and B can be expressed through new functions Φ and Ψ as follows:

$$A = (1 - \mathrm{e}^{-2a})[a\Psi + (1 + a)\Phi],$$

$$B = (1 - \mathrm{e}^{-2a})[(1 - a)\Psi - a\Phi]. \tag{24}$$

Substituting eqs (24) into eqs (14) and (15) and satisfying the boundary conditions on the crack surface (eq. 2), we obtain for $z = 0$ and $0 \leq r < 1$

$$\int_0^\infty \Big[\Phi - R_1(\xi h)\Phi - R_3(\xi h)\Psi\Big]J_0(\xi r)\xi d\xi = -\Delta p(r),$$

$$\int_0^\infty \Big[\Psi - R_2(\xi h)\Psi - R_3(\xi h)\Phi\Big]J_1(\xi r)\xi d\xi = \tau(r), \tag{25}$$

where $R_1(a) = (1 + 2a + 2a^2)\mathrm{e}^{-2a}$, $R_2(a) = (1 - 2a + 2a^2)\mathrm{e}^{-2a}$ and $R_3(a) = 2a^2\mathrm{e}^{-2a}$. Eqs (23) and (25) represent a system of dual integral equations for functions Φ and Ψ. These equations can be solved by expressing Φ and Ψ in terms of the following finite Fourier transforms:

$$\Phi(\xi) = \int_0^1 \sin \xi t\phi(t)dt,$$

$$\Psi(\xi) = \int_0^1 \left(\frac{\sin \xi t}{\xi t} - \cos \xi t\right)\psi(t)dt. \tag{26}$$

Substitutions (26) satisfy eqs (23) identically, while eqs (25) give rise to a pair of Schlömilch equations (Whittaker & Watson 1963), whose solutions are the following Fredholm equations of the second kind:

$$\phi(t) = -\frac{2}{\pi}\int_0^t \frac{\Delta p(r)rdr}{\sqrt{t^2 - r^2}} + \frac{2}{\pi}\int_0^1 \Big[T_1(t, r)\phi(r) + T_3(t, r)\psi(r)\Big]dr,$$

$$\psi(t) = \frac{2}{\pi t}\int_0^t \frac{\tau(r)r^2dr}{\sqrt{t^2 - r^2}} + \frac{2}{\pi}\int_0^1 \Big[T_2(t, r)\psi(r) + T_4(t, r)\phi(r)\Big]dr. \tag{27}$$

Closed-form expressions for the integration kernels T_{1-4} in eqs (27) are given in Appendix A. Eqs (27) can be solved numerically, for example, using a method of successive approximations (e.g. Delves & Mohamed 1985), whereby a solution is sought by iterating $\phi(t)$ and $\psi(t)$ using the right-hand sides of

eqs (27) until certain convergence criteria are met. As shown in Appendix A, kernels T_{1-4} are smooth bounded algebraic functions, which is essential for a numerical solution of eqs (27) [we note that the solution of Srivastava & Singh (1969) gives rise to kernels that are singular on the interval of integration]. Appendix A presents numerical solutions to a system (27) for a particular case of hydrostatic fluid pressure inside the crack. In the case of a non-hydrostatic stress distribution (for example, resulting from viscous flow of magma along the crack), coupled solutions for stresses at the crack walls and the concomitant host rock deformation may be obtained by adding another level of iterations to compute a viscous pressure drop that is consistent with the crack opening and the prescribed magma rheology (e.g. Fialko & Rubin 1999). Once the functions $\phi(t)$ and $\psi(t)$ are found, stresses and displacements in the half-space can be computed using formulae (12)–(19) after back-substituting $\phi(t)$ and $\psi(t)$ into eqs (26), and then eqs (26) into eqs (24).

4 DISPLACEMENTS OF THE EARTH'S SURFACE DUE TO A PENNY-SHAPED CRACK

Solutions for vertical and horizontal displacements at the free surface of a half-space can be obtained by putting $z = -h$ into eqs (12) and (13). Making use of the expressions (24), we obtain

$$U_z^s = 2(1 - v)\int_0^\infty \Big[(1 + \xi h)\Phi(\xi) + \xi h\Psi(\xi)\Big]\mathrm{e}^{-\xi h}J_0(\xi r)d\xi,$$

$$U_r^s = 2(1 - v)\int_0^\infty \Big[(1 - \xi h)\Psi(\xi) - \xi h\Phi(\xi)\Big]\mathrm{e}^{-\xi h}J_1(\xi r)d\xi. \tag{29}$$

Substituting eqs (26) into eqs (28) and (29) and changing the order of integration, we obtain final expressions for surface displacements in the form

$$U_j^s(r) = \int_0^1 \Big[K_\phi(r, t)\phi(t) + K_\psi(r, t)\psi(t)\Big]dt, \tag{30}$$

where $K_{\phi,\psi}$ are analytic kernels given in Appendix B. Computing surface displacements ultimately involves solving eqs (27) to find image functions $\phi(t)$ and $\psi(t)$, which are then used to calculate eq. (30). Fig. 2 compares maximum surface uplift due to a uniformly pressurized crack calculated using our solutions (see Appendix B) to an approximate analytic solution of Sun (1969) for a deep crack ($h \gg 1$) and an elastic solution for a thin circular plate with clamped edges (Landau & Lifshitz 1986). For large values of the non-dimensional crack depth ($h > 2$), the amplitude and shape of the surface uplift predicted by our solution are in an excellent agreement with the model and field experiments of Sun (1969), as well as with the point tensile dislocation model (Davis 1983). The discrepancy between our calculations and Sun's model for small h is probably due to the fact that in his model the boundary conditions on the crack surface are not satisfied exactly (see Section 2). For sufficiently small values of h, the amplitude of the maximum uplift produced by a penny-shaped crack is in a good qualitative agreement with a thin circular plate model (dashed line in Fig. 2). Fig. 3 shows profiles of vertical displacements of the free surface normalized by the maximum uplift for several values of h. For comparison we also plot the results of a finite element modelling of Dieterich & Decker (1975 models D and E in their Fig. 4). As one can see from Fig. 3, the differences between
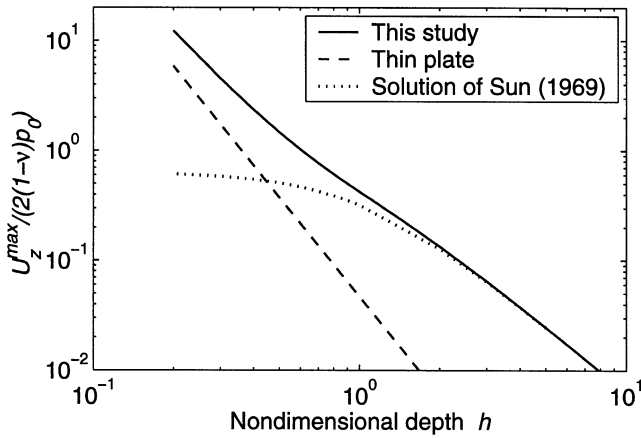
Figure 2. Maximum uplift of the free surface of a half-space produced by a penny-shaped crack (solid line) as a function of the non-dimensional crack depth h. In the limit $h \ll 1$, our model asymptotes to an analytic solution for a deflection of a uniformly loaded thin circular plate with clamped edges, $U_z^{\max} \propto h^4$ (Landau & Lifshitz 1986 p. 68) (dashed line). For $h \ll 1$, our model coincides with the approximate half-space solution of Sun (1969) (dotted line). Dimensional values of the maximum uplift can be obtained by multiplying the vertical axis by $2(1-v)R\Delta P/\mu$, where R is the crack radius and ΔP is the dimensional excess pressure inside the crack.

our semi-analytic solutions and the calculations of Dieterich & Decker are quite substantial. We have validated the accuracy of our model by numerical calculations using a 3-D boundary element code DIS3D (Rubin 1992; Fialko & Rubin 1999). The boundary element simulation of deformation due to a penny-shaped crack with $h = 0.5$, in which the crack has been approximated by ~900 square dislocations with prescribed constant-pressure boundary condition, has converged to the semi-analytic solution with a relative accuracy of a few per cent. We note that the finite element calculations of Dieterich & Decker (1975) agree reasonably with our solutions if the sill
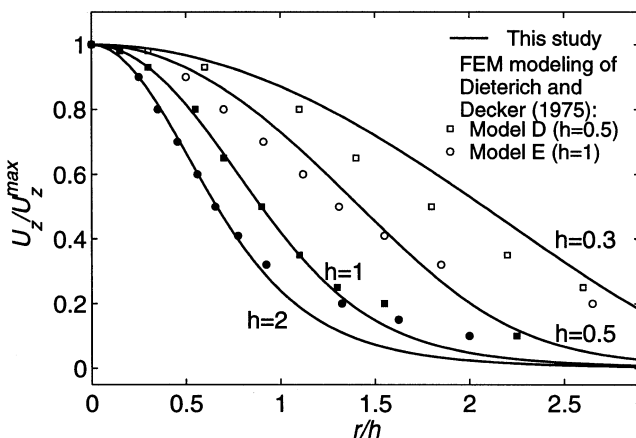

Figure 3. Profiles of vertical displacements of the free surface produced by a uniformly pressurized penny-shaped crack for several values of the non-dimensional crack depth h. Displacements are normalized by the maximum uplift value $U_z^{\max} = U_z^s(0)$ (see Fig. 2). The horizontal axis has units of the crack depth. Open symbols denote the finite element modelling results of Dieterich & Decker (1975 see their Fig. 4). Filled symbols denote the respective models of Dieterich & Decker rescaled assuming a doubled crack depth or a factor of two decrease in the crack radius (see text for details).
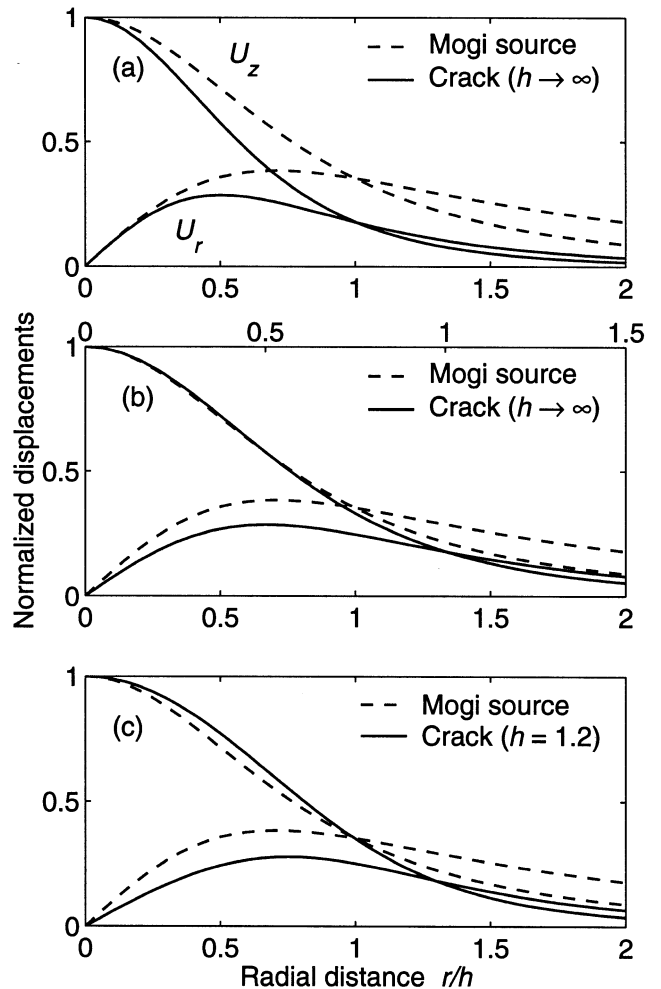
Figure 4. A comparison of surface displacements due to a spherically symmetric point source (Mogi model) and axially symmetric oblate source (penny-shaped crack). All displacements are normalized by the maximum vertical displacement $U_z^{\max}$. The horizontal axis represents radial distance from the source epicentre normalized by the source depth. (a) A Mogi source and a point crack at the same depth. (b) A Mogi source and a point crack that is $2/1.5 = 1.33$ times deeper than the Mogi source. Upper axis has units of the crack depth and lower axis has units of the Mogi source depth. (c) Mogi source and a finite crack ($h = 1.2$) at the same depth.

radii corresponding to models D and E of Dieterich & Decker are taken to represent the sill diameters (see filled symbols in Fig. 3).

Vertical and horizontal displacements of the free surface due to an axisymmetric oblate point source (that is, a crack with a large depth-to-radius ratio h) are appreciably different from those due to a spherically symmetric point source (Mogi 1958) at the same depth. Fig. 4(a) shows displacement profiles normalized by a maximum vertical displacement for the Mogi model and a point crack model (i.e. $h \gg 1$). As one can see from Fig. 4(a), a 'point crack' gives rise to more localized deformation than a 'point sphere'. Delaney & McTigue (1994) obtained a similar result by comparing the Mogi model to a tensile dislocation. Figs 4(b) and (c) illustrate various trade-offs between the source geometry and/or the source depth that produce nearly identical deformation patterns at the surface. In particular, surface displacements due to a pressurized spherical cavity may be essentially

similar to those due to a point crack ($h \gg 1$) at a greater depth (Fig. 4b) and a finite crack ($h \leq 1$) at the same (or shallower) depth (Fig. 4c). The main difference in surface displacements that potentially allows one to distinguish between the sill-like and pluton-like (i.e. more isometric) magma chamber geometries is a somewhat smaller ratio of maximum horizontal to maximum vertical displacements for sills ($U_r^{max}/U_z^{max} < 30$ per cent, Fig. 4) than for spherical sources ($U_r^{max}/U_z^{max} \sim 40$ per cent). Note that horizontal displacements alone are almost as insensitive to the trade-off between the source geometry and the source depth as vertical displacements are. Fig. 5 shows horizontal displacement profiles for the Mogi source (dashed line), a point crack (solid line) and a prolate cavity (dotted line) (Yang *et al.* 1988) normalized by U_r^{max}. As one can see from Fig. 5, the pattern of horizontal displacements due to a prolate spheroid and the Mogi source can be virtually identical. Horizontal oblate sources can potentially be distinguished from spherical or prolate sources due to a faster decay of surface displacements in the far field . However, decreasing displacement amplitudes in the far field imply a decrease in the signal-to-noise ratio. Given measurement errors and/or limited aperture of geodetic networks, differences seen in Figs 4 and 5 may be difficult to resolve by field observations.

For a crack model, the ratio of maximum horizontal displacements to maximum vertical displacements decreases with the non-dimensional crack depth h, as shown in Fig. 6. This result is expected, given that oblate sources are more efficient in generating vertical (rather than horizontal) displacements. Horizontal displacements in excess of 50 per cent of the maximum vertical displacement are usually thought to require an essentially prolate source geometry (Dieterich & Decker 1975; Yang *et al.* 1988). It should be borne in mind that the models discussed so far consider elastic deformation in a homogeneous isotropic medium. Relaxing one (or more) of the assumptions of elasticity, homogeneity and isotropy may affect the predicted
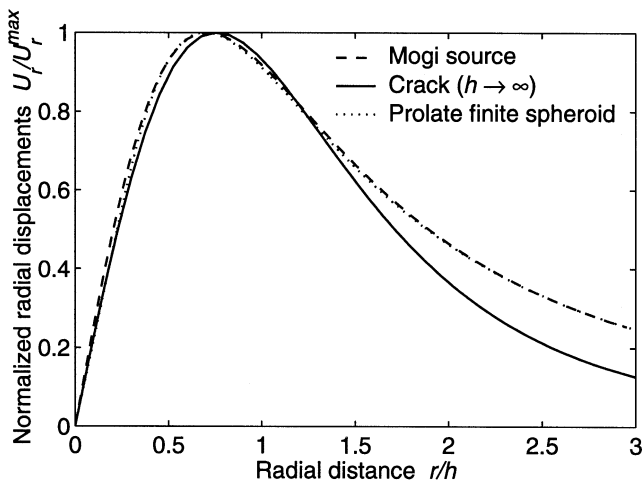

Figure 6. Ratio of maximum horizontal displacements to maximum vertical displacements as a function of the non-dimensional crack depth h. For cracks that are small compared to their depth, the ratio of maximum horizontal displacements to maximum vertical displacements is about 30 per cent.

deformation patterns. For example, as pointed out by Rubin (1992), a reasonable anisotropy of the elastic moduli of the upper crustal rocks may give rise to increases in the horizontal displacements relative to the vertical displacements of the order of several tens of per cent. Such an increase may result from reductions in the effective horizontal stiffness due to void opening in the presence of horizontal extension. Note that some horizontal extension is always produced in the overlying rocks as a result of magma chamber inflation. An increase in the ratio U_r^{max}/U_z^{max} of the order of several per cent to a few tens of per cent (compared to the isotropic half-space solutions) may also result from an increase in the effective elastic stiffness of the host rocks with depth (e.g. due to lithological stratification). Fig. 7 shows the effects of a step-like increase in the elastic rigidity on surface displacements due to the Mogi source.

Figure 5. A comparison of horizontal surface displacements due to a spherically symmetric point source (Mogi model), axially symmetric oblate point source (crack having $h \gg 1$) and axially symmetric finite prolate spheroid. The prolate spheroid has an axis aspect ratio of 3:1 and a ratio of the spheroid centre depth to the major axis of 5:3. All displacements are normalized by the maximum horizontal displacements, and distances from the source centre are given in units of the Mogi source depth. The point crack is 1.5 times deeper and the prolate spheroid 1.2 times shallower than the Mogi source.
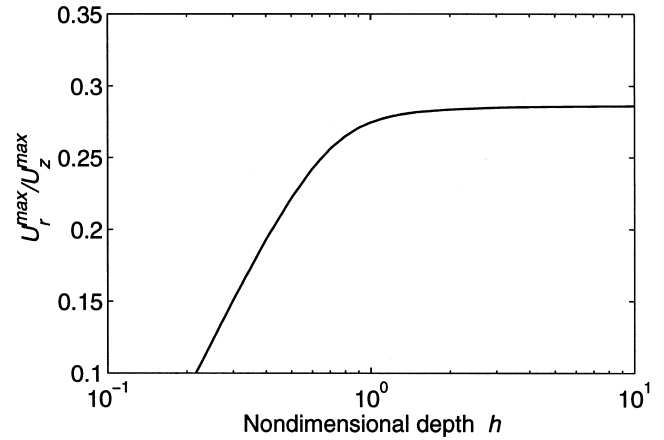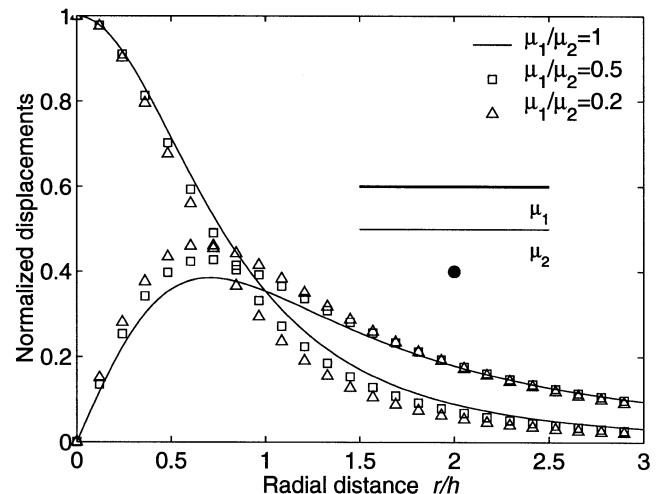

Figure 7. Theoretical surface displacements due to a spherical pressure source in a homogeneous half-space (Mogi model, solid line) and a two-layer half-space (symbols). The inset illustrates the geometry of the problem. A solid circle denotes an isotropic pressure source and μ_1 and μ_2 are the shear moduli of the upper and lower layers of a semi-infinite elastic body, respectively.

Increases in horizontal displacements relative to vertical displacements similar to those seen in Fig. 7 are also expected for other sources of dilation, including horizontal tensile cracks. For these reasons, interpretations of geodetic measurements of magma-induced deformation using isotropic models may be biased towards spherically symmetric or prolate sources.

5 VOLUME CHANGES DUE TO SILL INFLATION

An expression for a change in a sill volume ΔV due to a magma injection or withdrawal can be found using solutions for vertical displacements of the crack walls (eqs 21 for $r < 1$),

$$\Delta V = 2\pi \int_0^1 \left[U_z^{(2)}(r) - U_z^{(1)}(r) \right] r\,dr . \tag{31}$$

Eq. (31) describes a change in the crack volume that results from a pressure change inside the crack. Note that ΔV represents the volume of the injected/withdrawn fluid only if the fluid is incompressible; in the case of finite fluid compressibility, the crack volume change ΔV will generally underestimate a change in the fluid volume (e.g. Johnson *et al.* 2000). An explicit expression for ΔV is derived in Appendix C. Fig. 8 shows the results of numerical calculations for the crack volume change ΔV normalized by the crack volume change in an infinite elastic body $\Delta V(\infty)$ (solid line in Fig. 8) for a range of non-dimensional crack depths h. An increase in the ratio $\Delta V/\Delta V(\infty)$ with decreasing h reflects a decreasing resistance of the overlying strata to a crack opening for a given excess magma pressure. Also shown in Fig. 8 is the ratio of the volume of the lower part of the crack,

$$\Delta V^{(2)} = 2\pi \int_0^\infty U_z^{(2)}(r) r\,dr ,$$

to the total crack volume ΔV (dashed line). The ratio $\Delta V^{(2)}/\Delta V$ characterizes the asymmetry of deformation with respect to the crack plane, which is commonly used for defining a transition from a sill to a laccolith (e.g. Pollard & Holzhausen 1979).
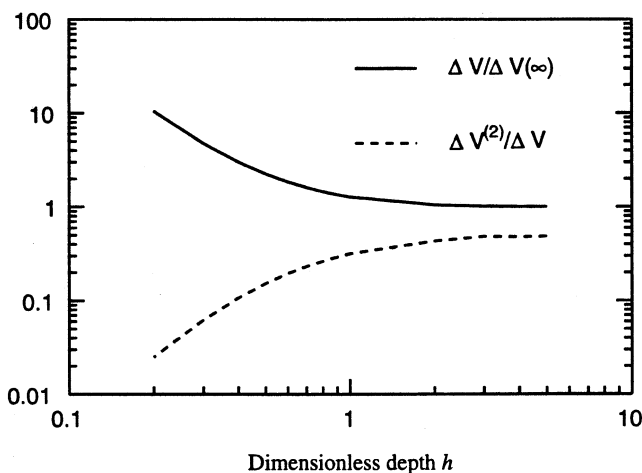

Figure 8. Dependence of the ratio of the total crack volume ΔV to the crack volume in an infinite elastic body $\Delta V(\infty)$ (solid line) and the ratio of the volume of the lower part of the crack to the total crack volume (dashed line) on the non-dimensional crack depth h. We assume hydrostatic pressure inside the crack (see Appendix C).

As one can see from Fig. 8, in a purely elastic model such a transition is expected to occur when $h \lesssim 1$. For $h \ll 1$, the deformation is essentially concentrated in the upper part of the crack. In Appendix C we also obtain an expression for the corresponding volume of the surface uplift (or subsidence, depending on the sign of the excess magma pressure inside the crack) and demonstrate that the surface uplift volume ΔV^s identically equals ΔV for any value of the crack depth-to-radius ratio h or the Poisson's ratio of the half-space v. Delaney & McTigue (1994) came to a similar conclusion using a horizontal dislocation model of Okada (1985). A one-to-one correspondence between ΔV^s and ΔV is perhaps surprising, as one might expect the ratio $\Delta V^s/\Delta V$ to be less than unity as h increases and the deformation becomes essentially symmetric with respect to the crack plane. This result provides a theoretical justification for using the volume of the surface uplift/subsidence as a direct measure of volume changes at the source for sill-like magma bodies.

6 CONCLUSIONS

We obtained exact solutions for stresses and displacements due to an arbitrarily loaded axisymmetric crack in an elastic half-space. These solutions may be used to investigate deformation of the Earth's surface associated with emplacement and growth of sill-like magma intrusions. A horizontal circular crack whose size is much smaller than its depth gives rise to a more localized surface deformation than does the Mogi source (i.e. a pressurized spherical cavity) located at the same depth. The deformation patterns produced by a Mogi source, a small crack at a larger depth, and a large crack at a shallower depth may be essentially similar. Small differences in surface displacements (in particular, in vertical displacements) due to various axisymmetric sources imply an intrinsic trade-off between the source geometry (e.g. oblate versus prolate) and the source depth in inversions of geodetic data. Interpretations of geodetic measurements of only one component of deformation (either vertical or horizontal) are particularly vulnerable to this trade-off. The use of homogeneous elastic half-space models may bias the interpretation of geodetic data towards spherical or prolate source geometries if the host rocks exhibit non-linear elastic and/or transversely isotropic mechanical properties. We explicitly relate variations in the excess magma pressure inside a sill intrusion to changes in the intrusion volume. We show that the volume of inflation (or deflation) of a magma sill exactly equals the volume of the resulting uplift (or subsidence) at the Earth's surface for any values of the sill depth-to-radius ratio h and the Poisson's ratio of the host rocks v. Therefore, the volume of the surface uplift inferred from field observations may be used as a direct proxy for the volume increase of sill-like intrusions during episodes of magmatic inflation.

from the authors. Contribution number 8707 of the Division of Geological and Planetary Sciences, Seismological Laboratory, California Institute of Technology.

REFERENCES

Abramowitz, M. & Stegun, I., 1972. *Handbook of Mathematical Functions with Formulas, Graphs and Mathematical Tables,* US Govt. Printing Office, Washington, DC.

Anderson, E.M., 1938. The dynamics of sheet intrusion, *Proc. R. Soc. Edinburgh,* **B58,** 242–251.

Bianchi, R., Coradini, A., Federico, C., Giberti, G., Lanciano, P., Pozzi, J., Sartoris, G. & Scadrone, R., 1987. Modeling of surface deformation in volcanic areas: the 1970–1972 and 1982–1984 crises at Campi Flegrei, Italy, *J. geophys. Res.,* **92,** 14 139–14 150.

Davis, P.M., 1983. Surface deformation associated with a dipping hydrofracture, *J. geophys. Res.,* **88,** 5826–5834.

Davis, P.M., 1986. Surface deformation due to inflation of an arbitrarily oriented triaxial ellipsoidal cavity in an elastic half-space, with reference to Kilauea Volcano, Hawaii, *J. geophys. Res.,* **91,** 7429–7438.

Delaney, P.T. & McTigue, D.F., 1994. Volume of magma accumulation or withdrawal estimated from surface uplift or subsidence, with application to the 1960 collapse of Kilauea Volcano, *Bull. Volcanol.,* **56,** 417–424.

Delves, L. & Mohamed, J., 1985. *Computational Methods for Integral Equations,* Cambridge University Press, New York.

Dieterich, J. & Decker, R., 1975. Finite element modeling of surface deformation associated with volcanism, *J. geophys. Res.,* **80,** 4094–4102.

Dvorak, J. & Dzurisin, D., 1997. Volcano geodesy: the search for magma reservoirs and the formation of eruptive vents, *Rev. Geophys.,* **35,** 343–384.

Dzurisin, D. & Yamashita, K., 1987. Vertical surface displacements at Yellowstone caldera, Wyoming, 1976–1986, *J. geophys. Res.,* **92,** 13 753–13 766.

Fialko, Y.A. & Rubin, A.M., 1999. What controls the along-strike slopes of volcanic rift zones?, *J. geophys. Res.,* **104,** 20 007–20 020.

Fialko, Y. & Simons, M., 2000. Deformation and seismicity in the Coso geothermal area, Inyo County, California: observations and modeling using satellite radar inteferometry, *J. geophys. Res.,* **105,** 21 781–21 793.

Fialko, Y., Simons, M. & Khazan, Y., 2001. Finite source modelling of magmatic unrest in Socorro, New Mexico, and Long Valley, California, *Geophys. J. Int.,* **146,** 191–200 (this issue).

Gradshteyn, I.S. & Ryzhik, I.M., 1994. *Table of Integrals, Series, and Products,* 5th edn, Academic Press, San Diego.

Gudmundsson, A., 1986. Possible effect of aspect ratios of magma chambers on eruption frequency, *Geology,* **14,** 991–994.

Guterman, V.G., Fialko, Y.A. & Khazan, Y.M., 1996. Dome structures over sill-like crustal structures: a numerical model of preseismic uplift. 1. *Geophys. J.,* **16,** 209–226. (English transl.).

Guterman, V.G., Fialko, Y.A. & Khazan, Y.M., 1997. Dome structures over sill-like crustal structures: a numerical model of preseismic uplift. 2. *Geophys. J.,* **16,** 543–554. (English transl.).

Johnson, D.J., Sigmundsson, F. & Delaney, P.T., 2000. Comment on 'Volume of magma accumulation or withdrawal estimated from surface uplift or subsidence, with application to the 1960 collapse of Kilauea Volcano' by P.T. Delaney & D.F. McTigue, *Bull. Volcanol.,* **61,** 491–493.

Khazan, Y.M. & Fialko, Y.A., 1995. Fracture criteria at the tip of fluid driven cracks in the Earth, *Geophys. Res. Lett.,* **22,** 2541–2544.

Kuzmin, Y.A. & Uflyand, Y.S., 1965. Axisymmetric elastic problem for a half-space weakened by a flat circular slit, *Appl. Math. Mech.,* **29,** 1132–1137.

Lanari, R., Lundgren, P. & Sansosti, E., 1998. Dynamic deformation of Etna volcano observed by satellite radar interferometry, *Geophys. Res. Lett.,* **25,** 1541–1544.

Landau, L.D. & Lifshitz, E.M., 1986. *Theory of Elasticity,* Pergamon Press, Oxford.

Linde, A., Agustsson, Sacks, K.I. & Stefansson, R., 1993. Mechanism of the 1991 eruption of Helka from continuous borehole strain monitoring, *Nature,* **365,** 737–740.

McTigue, D.F., 1987. Elastic stress and deformation near a finite spherical magma body: resolution of the point source paradox, *J. geophys. Res.,* **92,** 12 931–12 940.

Mogi, K., 1958. Relations between the eruptions of various volcanoes and the deformations of the ground surfaces around them, *Bull. Earthq. Res. Inst. Univ. Tokyo,* **36,** 99–134.

Okada, Y., 1985. Surface deformation due to shear and tensile faults in a half-space, *Bull. seism. Soc. Am.,* **75,** 1135–1154.

Pollard, D.D., 1973. Derivation and evaluation of a mechanical model for sheet intrusions, *Tectonophysics,* **19,** 233–269.

Pollard, D.D. & Holzhausen, G., 1979. On the mechanical interaction between a fluid-filled fracture and the Earth's surface, *Tectonophysics,* **53,** 27–57.

Pollard, D.D. & Segall, P., 1987. Theoretical displacements and stresses near fractures in rock: with applications to faults, joints, veins, dikes, and solution surfaces, in *Fracture Mechanics of Rock,* pp. 277–349, ed. Atkinson, B.K., Academic Press, San Diego.

Rubin, A.M., 1992. Dike-induced faulting and graben subsidence in volcanic rift zones, *J. geophys. Res.,* **97,** 1839–1858.

Savage, J.C., Cockerham, R.S., Estrem, J.E. & Moore, L.R., 1987. Deformation near the Long Valley caldera, eastern California, 1982–1986, *J. geophys. Res.,* **92,** 2721–2746.

Sneddon, I.N., 1951. *Fourier Transforms,* McGraw-Hill, New York.

Srivastava, K.N. & Singh, K., 1969. The effect of penny-shaped crack on the distribution of stress in a semi-infinite solid, *Int. J. Eng. Sci.,* **7,** 469–490.

Sun, R.J., 1969. Theoretical size of hydraulically induced horizontal fractures and corresponding surface uplift in an idealized medium, *J. geophys. Res.,* **74,** 5995–6011.

Whittaker, E.T. & Watson, G.N., 1963. *A Course of Modern Analysis; an Introduction to the General Theory of Infinite Processes and of Analytic Functions,* Cambridge University Press, Cambridge.

Wu, M. & Wang, H.F., 1988. Deformations and inferred stress-field for ellipsoidal sources at Long Valley, California, 1975–1982, *J. geophys. Res.,* **93,** 13 285–13 296.

Yang, X.-M., Davis, P.M. & Dieterich, J.H., 1988. Deformation from inflation of a dipping finite prolate spheroid in an elastic half-space as a model for volcanic stressing, *J. geophys. Res.,* **93,** 4249–4257.

APPENDIX A: SOLUTIONS TO FREDHOLM EQUATIONS FOR THE CASE OF A UNIFORMLY PRESSURIZED PENNY-SHAPED CRACK

For a hydrostatic pressure distribution inside a penny-shaped crack, $\Delta p(r) = \text{const} = p_0$, and $\tau(r) = 0$, integral equations (27) give rise to the following system of equations for normalized functions $\bar{\phi}(t) = \phi(t)/p_0$ and $\bar{\psi}(t) = \psi(t)/p_0$:

$$\bar{\phi}(t) = -\frac{2t}{\pi} + \frac{2}{\pi}\int_0^1 \left[T_1(t, r)\bar{\phi}(r) + T_3(t, r)\bar{\psi}(r)\right]dr,$$

$$\bar{\psi}(t) = \frac{2}{\pi}\int_0^1 \left[T_2(t, r)\bar{\psi}(r) + T_4(t, r)\bar{\phi}(r)\right]dr. \tag{A1}$$

Kernels T_{1-4} in eqs (A1) are smooth bounded functions on the interval of integration,

$$T_1(t, r) = \int_0^\infty R_1(\xi h) \sin \xi t \sin \xi r d\xi$$

$$= 4h^3 \Big[P_1(t - r) - P_1(t + r) \Big], \qquad \text{(A2)}$$

$$T_2(t, r) = \int_0^\infty R_2(\xi h) \Big(\frac{\sin \xi t}{\xi t} - \cos \xi t \Big) \Big(\frac{\sin \xi r}{\xi r} - \cos \xi r \Big) d\xi$$

$$= \frac{h}{tr} \Big[P_2(t - r) - P_2(t + r) \Big] + h \Big[P_3(t - r) + P_3(t + r) \Big], \qquad \text{(A3)}$$

$$T_3(t, r) = \int_0^\infty R_3(\xi h) \sin \xi t \Big(\frac{\sin \xi r}{\xi r} - \cos \xi r \Big) d\xi$$

$$= \frac{h^2}{r} \Big[P_4(t - r) - P_4(t + r) - 2r \big((t - r) P_1(t - r)$$

$$+ (t + r) P_1(t + r) \big) \Big], \qquad \text{(A4)}$$

$$T_4(t, r) = T_3(r, t), \qquad \text{(A5)}$$

where expressions for R_{1-3} are given by eqs (25) and

$$P_1(x) = \frac{12h^2 - x^2}{(4h^2 + x^2)^3},$$

$$P_2(x) = \ln(4h^2 + x^2) + \frac{8h^4 + 2x^2h^2 - x^4}{(4h^2 + x^2)^2},$$

$$P_3(x) = 2 \frac{8h^4 - 2x^2h^2 + x^4}{(4h^2 + x^2)^3},$$

$$P_4(x) = \frac{4h^2 - x^2}{(4h^2 + x^2)^2}.$$

Eqs (A1) are solved numerically using a method of successive approximations (e.g. Delves & Mohamed 1985). The method is robust for values of the non-dimensional crack depth $h > 0.2$; convergence of the iterated kernel series degrades as h decreases, and the method becomes inapplicable for $h \leq 0.18$. Numerical integration is performed by subdividing the interval of integration into four equal intervals and using a 16-point Gaussian quadrature (Abramowitz & Stegun 1972) on each interval. Iterations start with the initial guesses $\bar{\phi}(t) = -2t/\pi$ and $\bar{\psi}(t) = 0$ corresponding to a full-space solution (i.e. $h \to \infty$) and continue until solutions converge within six significant figures. Fig. A1 shows solutions to a system (A1) for several values of h. We note that coefficients $\bar{\phi}(1)$ and $\bar{\psi}(1)$ represent non-dimensional stress intensity factors at the crack tips of modes I and II, respectively (Srivastava & Singh 1969; Guterman *et al.* 1997).

APPENDIX B: SEMI-ANALYTIC EXPRESSIONS FOR SURFACE DISPLACEMENTS

Substitution of eqs (26) into eqs (28) and (29) gives rise to the following expressions for surface displacements U_z^s and U_r^s (for simplicity, we assume hydrostatic pressure p_0 inside the crack, see Appendix A; solutions for an arbitrary stress distribution
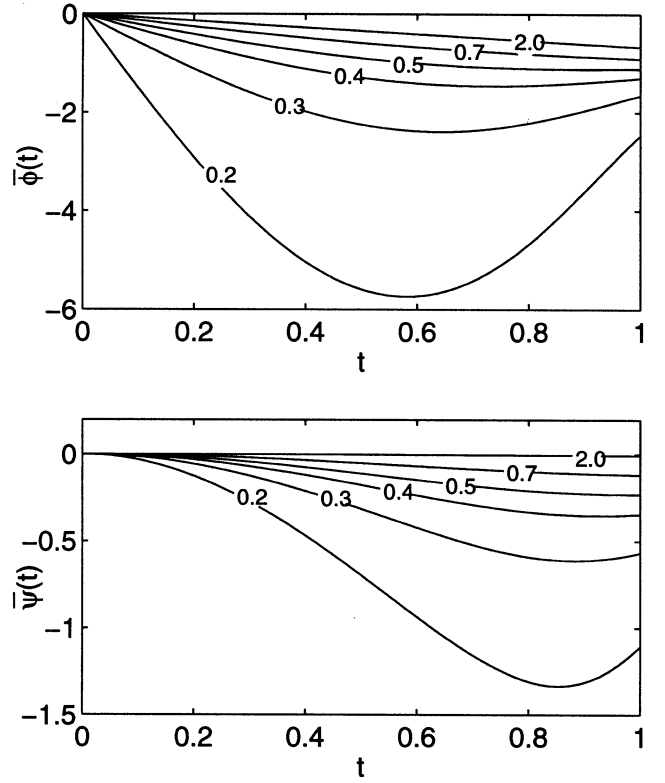
Figure A1. Numerical solutions to eqs (A1) for several values of the crack depth-to-radius ratio h (labelled).

on the crack surface can be derived using the same formalism):

$$\frac{U_z^s}{2(1 - v)p_0} = \int_0^1 \Big[S_0^0 + h S_0^1 \Big] \bar{\varphi}(t) dt + \int_0^1 \Big[\frac{S_0^0}{t} - C_0^1 \Big] \bar{\psi}(t) dt, \quad \text{(B1)}$$

$$\frac{U_r^s}{2(1 - v)p_0} = \int_0^1 \Big[\frac{S_1^{-1} - h S_1^0}{t} - C_1^0 + h C_1^1 \Big] \bar{\psi}(t) dt - h \int_0^1 S_1^1 \bar{\varphi}(t) dt, \qquad \text{(B2)}$$

where we denote

$$S_m^n(r, t; h) = \int_0^\infty \xi^n e^{-\xi h} J_m(\xi r) \sin(\xi t) d\xi, \qquad \text{(B3)}$$

$$C_m^n(r, t; h) = \int_0^\infty \xi^n e^{-\xi h} J_m(\xi r) \cos(\xi t) d\xi. \qquad \text{(B4)}$$

Evaluation of improper integrals (B3)–(B4) yields the following closed-form expressions (Gradshteyn & Ryzhik 1994, pp. 734–735):

$$S_0^0 = \frac{\sqrt{2} h t}{X_2 \sqrt{X_2 + X_1}}, \qquad \text{(B5)}$$

$$S_0^1 = \frac{h \sqrt{X_2 - X_1}(2X_1 + X_2) - t \sqrt{X_2 + X_1}(2X_1 - X_2)}{\sqrt{2} X_2^3}, \quad \text{(B6)}$$

$$C_0^1 = \frac{h \sqrt{X_2 + X_1}(2X_1 - X_2) + t \sqrt{X_2 - X_1}(2X_1 + X_2)}{\sqrt{2} X_2^3},$$

$$S_1^{-1} = \frac{t}{r} - \frac{\sqrt{X_2 - X_1}}{\sqrt{2} r}, \qquad \text{(B8)}$$

$$S_1^0 = \frac{t\sqrt{X_2 + X_1} - h\sqrt{X_2 - X_1}}{\sqrt{2}rX_2} \,, \tag{B9}$$

$$C_1^0 = \frac{1}{r} - \frac{h\sqrt{X_2 + X_1} + t\sqrt{X_2 - X_1}}{\sqrt{2}rX_2} \,, \tag{B10}$$

$$C_1^1 = \frac{r\sqrt{X_2 + X_1}(2X_1 - X_2)}{\sqrt{2}X_2^3} \,, \tag{B11}$$

$$S_1^1 = \frac{r\sqrt{X_2 - X_1}(2X_1 + X_2)}{\sqrt{2}X_2^3} \,. \tag{B12}$$

In eqs (B5)–(B12),

$$X_1 = h^2 + r^2 - t^2, \quad X_2 = \sqrt{X_1^2 + 4h^2t^2} \,. \tag{B13}$$

The results of calculations for U_z^s and U_r^s using expressions given in Appendices A and B are shown in Figs 2–4.

APPENDIX C: INTRUSION VOLUME CHANGE ΔV AND THE ASSOCIATED SURFACE UPLIFT VOLUME ΔV^S

After substituting expressions (21) and (22) into (31), we obtain the following equation for the intrusion volume change ΔV:

$$\Delta V = -4\pi(1 - v)\int_0^1 rdr \int_0^\infty \Phi(\xi)J_0(\xi r)d\xi \,. \tag{C1}$$

Integration over r yields

$$\frac{\Delta V}{4\pi(1 - v)} = -r\int_0^\infty \Phi(\xi)J_1(\xi r)\frac{d\xi}{\xi}\Big|_{r=0}^{r=1}$$

$$= -\int_0^\infty \Phi(\xi)J_1(\xi)\frac{d\xi}{\xi} \,, \tag{C2}$$

where $I|_a^b = I(b) - I(a)$ denotes evaluation at integration limits. Making a substitution (26) and assuming that the crack is held open by a hydrostatic excess pressure p_0 (see Appendix A), we obtain

$$\frac{\Delta V}{4\pi(1 - v)p_0} = -\int_0^1 dt\bar{\varphi}(t)\int_0^\infty \sin(\xi t)J_1(\xi)\frac{d\xi}{\xi} \,. \tag{C3}$$

In eq. (C3), an improper integral over ξ has the form of eq. (B3) (with $n = -1$, $m = 1$, $h = 0$, $r = 1$), and from eq. (B8) one can infer that

$$\int_0^\infty \sin(\xi t)J_1(\xi)\frac{d\xi}{\xi} = t \tag{C4}$$

(note that in eq. B8 $X_2 - X_1 = 0$ for $h = 0$; see eqs B13). Thus, we finally obtain

$$\frac{\Delta V}{4\pi(1 - v)p_0} = -\int_0^1 t\bar{\varphi}(t)dt \,. \tag{C5}$$

For a particular case of $h \to \infty$ (that is, for a crack in an infinite elastic body), $\bar{\varphi}(t) = -2t/\pi$ (see Fig. A1), and from eq. (C5) the corresponding crack volume is $\Delta V(\infty) = 8(1 - v)p_0/3$. Multiplying this result by a dimensional factor R^3, where R is the crack radius, and recalling that p_0 represents the ratio of the dimensional excess fluid pressure to shear modulus of the medium, we retrieve an analytic solution for a volume of a uniformly pressurized penny-shaped crack in an infinite elastic body (e.g. Sneddon 1951, p. 491). The ratio $\Delta V(h)/\Delta V(\infty)$ is shown in Fig. 8.

An expression for the associated volume of uplift of the half-space surface can be found in a similar way,

$$\Delta V^s = -2\pi\int_0^\infty U_z^s(r)rdr \,. \tag{C6}$$

Putting an expression for U_z^s (eq. 28) into eq. (C6) and changing the order of integration, we obtain

$$\frac{\Delta V^s}{4\pi(1 - v)} = -\lim_{r\to\infty} r\int_0^\infty \Big[(1 + \xi h)\Phi(\xi) + \xi h\Psi(\xi)\Big]e^{-\xi h}J_1(\xi r)\frac{d\xi}{\xi} \,. \tag{C7}$$

Utilizing the results presented in Appendix B for a uniformly pressurized crack, expression (C7) gives rise to

$$\frac{\Delta V^s}{4\pi(1 - v)p_0} = -\lim_{r\to\infty} r\int_0^1 dt\Big(\Big[S_1^{-1} + hS_1^0\Big]\bar{\varphi}(t)$$

$$+ \Big[\frac{S_1^{-1}}{t} - C_1^0\Big]\bar{\psi}(t)\Big) \,. \tag{C8}$$

It is straightforward to show using expressions (B8)–(B10) and (B13) that

$$\lim_{r\to\infty} rS_1^{-1} = t \,, \tag{C9}$$

$$\lim_{r\to\infty} rS_1^0 \equiv 0 \,, \tag{C10}$$

$$\lim_{r\to\infty} rC_1^0 \equiv 1 \,. \tag{C11}$$

Thus, eq. (C8) reduces to

$$\frac{\Delta V^s}{4\pi(1 - v)p_0} = -\int_0^1 t\bar{\varphi}(t)dt \,. \tag{C12}$$

Comparing eqs (C12) and (C5), we deduce that $\Delta V^s/\Delta V \equiv 1$ for any values of the non-dimensional crack depth h and the Poisson's ratio v of an elastic half-space. Delaney & McTigue (1994) arrived at the same conclusion using elastic solutions for a horizontal rectangular dislocation. We note that our result for sill-like magma bodies holds for any axisymmetric distribution of stresses on the sill surface. For the Mogi source $\Delta V^s/\Delta V = 2(1 - v)$, that is, for compressible rocks the volume of surface uplift may exceed the volume increase at the source by more than 50 per cent (Delaney & McTigue 1994).